Eur. Phys. J. B **49**, 407–414 (2006)
DOI: 10.1140/epjb/e2006-00092-2

THE EUROPEAN PHYSICAL JOURNAL B

Electron mobility in a modulation doped AlGaN/GaN quantum well

Z. Yarar[1], B. Ozdemir[2], and M. Ozdemir[2,a]

[1] Department of Physics, Faculty of Arts and Sciences, Mersin University, Çiftlikköy 33343 Mersin, Turkey
[2] Department of Physics, Cukurova University, 01330 Adana, Turkey

Received 14 November 2005
Published online 31 March 2006 –

Abstract. We consider a two dimensional electron gas confined to a modulation doped AlGaN/GaN quantum well and study the dependence of low field mobility on various parameters such as composition, well width, remote impurity and interface roughness as a function of temperature. GaN is assumed to be in the zincblende structure. Acoustic and optical phonon, ionized remote impurity and interface roughness scatterings are taken into account in mobility calculations. The scattering rates are calculated using the self-consistently calculated wave functions obtained from the numerical solution of Poisson and Schrödinger equations. Also found from the self-consistent solutions are the potential profile at the junction, the energy levels in the well and electron concentrations in each level. Ensemble Monte Carlo method is used to find the drift velocities of the two dimensional electrons along the interface under an applied field. The mobility of two dimensional electrons is obtained from the drift velocity of electrons. It is found that while remote impurity scattering is very effective for small values of spacer layer and doping concentrations, increasing Al concentration reduces the mobility of electrons. The effect of surface roughness, on the other hand, on mobility is almost independent of well width. The results of our simulations are compatible with the existing experimental data.

PACS. 72.20.Dp General theory, scattering mechanisms – 72.20.Fr Low-field transport and mobility; piezoresistance – 73.40.Kp III-V semiconductor-to-semiconductor contacts, p-n junctions, and heterojunctions

1 Introduction

High energy gap materials have been the subject of intensive investigation for the past decade due to their superior properties such as high electron mobility, high heat conductivity and high breakdown voltage compared to conventionally used materials like GaAs [1–30]. These N containing materials (GaN, AlN and InN) known as III-nitride semiconductors are also good candidates for the fabrication of devices working in blue and ultraviolet regimes of spectrum. Besides, they have high electron mobilities and high heat conductivities [1–3].

Materials having different band gap energies are used to obtain hetero structures to manufacture devices based on these semiconductor structures, an idea suggested long ago [4] and confirmed soon after [5]. In these selectively doped semiconductor hetero structures a two dimensional electron gas forms at the hetero interface which is usually separated from the impurities on the high energy gap side by a thin layer of undoped material. This separation reduces the scattering of electrons due to donor impurities and hence improves the mobility of the electrons especially at low field and temperature values. In this context, AlGaN/GaN hetero structures are good candidates for high power and high frequency amplifying devices for communication and for other applications such as detectors. Moreover AlGaN/GaN field effect transistors have better operating characteristics at high power and high temperatures compared to for example previously used AlGaAs/GaAs structures.

GaN is usually grown on sapphire substrate and crystallizes in wurtzite phase. Under certain conditions GaN also crystallizes in zincblende lattice on substrates having zincblende structure [6]. Wurtzite type GaN have strong piezoelectric and spontaneous polarization properties and therefore large polarization fields develop at the hetero interfaces of AlGaN/GaN hetero structures which causes further band bending at the junction and hence lead to enhanced confined charge accumulation at the interface [7–14]. Because of the band offset between AlGaN and GaN, these electrons are free to move on the plane of the hetero interface but are restricted in the direction

[a] e-mail: metoz@cu.edu.tr

perpendicular to the interface (growth direction). For this reason the electron charge confined at the hetero interface is known as a quasi two dimensional electron gas (2DEG). Because of the high band offset value at the junction and polarization effects just mentioned, very high two dimensional electron concentrations can be obtained in this structure even in the absence of any intentional impurity doping [15,16].

In zincblende type GaN, on the other hand, spontaneous and piezoelectric field inductions are less pronounced. In the present work we neglect spontaneous and piezoelectric fields and study the electron transport properties in a fully relaxed modulation doped AlGaN/GaN quantum well using ensemble Monte Carlo technique. We, however, use the material parameters for wurtzite type GaN for zincblende structure, since most of the parameter values for these two types used in this study are close to each other as pointed out in reference [31]. A similar study is carried out by the present authors for a similarly structured quantum well where modulation doping and remote impurity scattering were neglected [17].

Charge confinement at the hetero junction, the transport of these two dimensional electrons and the mobility of these electrons have been intensively investigated for III-nitride semiconductor hetero structures in the past decade by many workers in the field [7–30].

In the present work we study the low field transport properties of two dimensional electrons confined to AlGaN/GaN modulation doped quantum well as a function of temperature, well width, spacer length and the roughness of the hetero interface. The drift velocity of carriers, the occupation of energy levels in 2D are calculated by an ensemble Monte Carlo technique. Electron mobility as a function of temperature is obtained for various values of well width, remote impurities, composition, surface roughness and spacer length. Scattering processes that are taken into account are acoustic and optical phonon scattering, remote impurity scattering and interface roughness scattering. The scattering rates are calculated using the wave functions obtained from the self consistent solution of Schrödinger and Poisson equations. Emphasis is given to the role of surface roughness scattering, well width, spacer length, Al composition and donor concentration on electron mobility. An exponential autocorrelation function is used to model the interface roughness scattering. The agreement between simulated and some experimental results are quite satisfactory.

The organization of the paper is as follows: Section 2 gives a concise summary of band gap structure for used in the calculations the hetero junction under consideration. In addition to material parameters used in the simulations, adequate references for the self consistent numerical solution of Poisson-Schrödinger equations and the scattering rates due to acoustic and optical phonons, ionized remote impurities and interface roughness are provided in this section. In Section 3 the main results of the Monte Carlo transport properties of 2D electrons and their discussions are presented. This section is devoted to the calculation of electron velocities and electron mobilities at various temperatures for various quantum well widths, Al concentrations, spacer length and surface roughness parameters. A summary and conclusions are presented in Section 4.

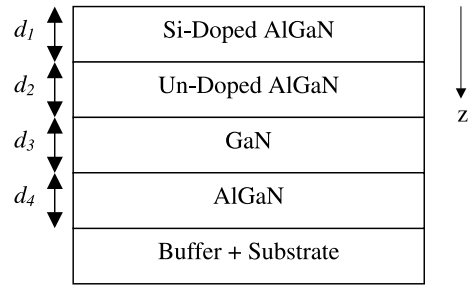

Fig. 1. A typical geometry of the sample used in the simulations.

2 Theory

The geometry of a typical modulation doped $Al_xGa_{1-x}N$/GaN quantum well hetero structure and doping profiles used in this study is shown in Figure 1. z-axis is chosen to be the growth axis. The Schrödinger equation in the effective mass and Hartree approximations for a single electron [32] and the Poisson equation for the quantum well under consideration are numerically solved self consistently at a given temperature and for a given distribution of donor and acceptor impurities. The variation of effective mass with respect to Al fraction in GaN is not considered, they are assumed to be equal to the effective mass of electrons in the Γ valley of GaN. The static dielectric constant in AlGaN layers is taken to be the value that corresponds to AlN (see Tab. 1). The two equations just mentioned are discretized using finite difference approximations for derivatives [33,34]. We assume that the Fermi level is pinned at a value of 1 eV on the barrier side below the conduction band of the AlGaN. On the substrate side the electric field in the AlGaN is assumed to vanish everywhere. Al mole fractions of $x = 0.15$, 0.2 and 0.3 are used in the calculations. Under these circumstances the 1 eV value chosen for Fermi level corresponds to 0.84 eV Ni Schottky barrier of the cap material grown on the top of the AlGaN layer on the barrier side. For more details of self consistent calculation see [17]. The conduction band discontinuity at the AlGaN/GaN junction is assumed to be in the form [8,35]

$$\Delta E_c = 0.75[E_g(x) - E_g(0)] \tag{1}$$

where $E_g(x)$ is the Al fraction (x) dependent gap energy assumed to be linearly interpolated between the the gap energy of GaN and that of AlN. It is assumed to be of the form [18]

$$E_g(x) = xE_g(\mathrm{AlN}) + (1-x)E_g(\mathrm{GaN}) \tag{2}$$

where $E_g(\mathrm{AlN})$ and $E_g(\mathrm{GaN})$ are the band gaps of AlN and GaN, respectively (see Tab. 1). From the solutions

Table 1. Material parameters used in the mobility calculation for $Al_{0.3}Ga_{0.7}N$/GaN quantum well structure. Only the parameters that are used in simulations are shown for AlGaN. For further details for parameters see [31,48].

	Unit	GaN	$Al_{0.3}Ga_{0.7}N$
Mass density ρ	kg/m^3	6.15×10^{3} [a]	...
Effective mass	m_0	0.2 [b]	0.2
Static dielectric constant ϵ_s	ϵ_0	8.9 [c]	8.5 [a]
Optical dielectric constant ϵ_∞	ϵ_0	5.35 [c]	...
Elastic constant c_L	N/m^2	2.65×10^{11} [a]	
LO-phonon energy	meV	91.2 [a]	...
Inter valley phonon energy	meV	91.2 [a]	...
Acoustic phonon velocity $(c_L/\rho)^{1/2}$	m/s	6.56×10^{3}	...
Deformation potential D	eV	8.3 [a]	...
Inter valley deformation pot. (equivalent and non-equiv.) D_{ij}	eV/m	1×10^{11} [*]	...
Band gap	eV	3.4	4.24 [d]
Other parameters	Unit		
Ni Schottky barrier	eV		0.84 [d]
Band offset ΔE_c	eV		$0.75[E_g(x) - E_g(0)]$ [e]

[a]: Reference [49]; [b]: reference [1]; [c]: reference [31]; [d]: reference [3]; [e]: reference [8,35]. [*]: Assumed to be equal to GaAs value.

of Poisson and Schrödinger equations the number of occupied or empty states in the quantum well, the electron concentration in each level, the wave functions and energy eigen values corresponding to each level are obtained at a given temperature.

A typical conduction band energy profile and the first two eigen functions for a quantum well that corresponds to the geometry shown in Figure 1 is depicted in Figure 2 when the temperature is $T = 77$ K. The parameters of the hetero junction are as follows (see Fig. 1): $d_1 = 152$ Å, $d_2 = 52$ (spacer) Å, $d_3 = 80$ Å and $d_4 = 300$ Å. The donor concentration in the AlGaN layer is $N_d = 6 \times 10^{24}$ m^{-3}, the other regions are undoped and acceptor impurity $N_A = 0$ everywhere. The first three sub band energy values measured with respect to conduction band minima are: 0.111, 0.177 and 0.281 eV. Only the first two sub bands are populated by electrons and the electron concentrations in these two levels are calculated to be 2.3×10^{12} cm^{-2} and 1.6×10^{9} cm^{-2}, respectively. Since the Poisson and Schrödinger equations are solved at the heterojunction using the impurity doping profile, the calculated electron density and the assumed donor impurity density are related, they are not independent parameters.

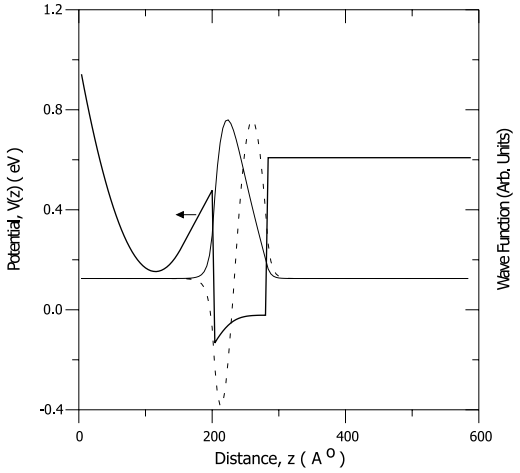

Fig. 2. The conduction band structure (left axis) corresponding to a sample geometry shown in Figure 1 at $T = 77$ K where $d_1 = 152$ Å, $d_2 = 52$ Å, $d_3 = 80$ Å and $d_4 = 300$ Å. The zero of energy scale corresponds to Fermi energy. The donor concentration in the AlGaN layer is $N_D = 6\times10^{24}$ m^{-3}, $N_A = 0$ everywhere and the other regions are undoped. The sub band energy values measured with respect to conduction band minima are: 0.111, 0.177 and 0.281 eV. Only the first two sub bands are populated by electrons and their densities are 2.3×10^{12} cm^{-2} and 1.6×10^{9} cm^{-2}, respectively. Also shown are the wave functions (right axis) corresponding to ground (solid line) and first excited (dashed line) states.

Once the electron wave functions are known, the scattering rates due to various mechanisms can be calculated. The scattering processes that are included in our calculations in 2D are as follows: acoustic and optical phonon [36–38] remote impurity [32,39,40] and surface roughness [40–44] scattering. Acoustic phonon scattering in two dimensions is calculated using the wave functions generated from the Poisson-Schrödinger solution [37]. Acoustic phonon scattering is assumed to be elastic and the thermal energy k_BT_L where k_B is Boltzmann's constant and T_L is the lattice temperature is assumed to be much higher than the acoustic phonon energies. Longitudinal optical phonon scatterings are also calculated using the wave functions found from the self consistent solutions for the two dimensional electrons and their scattering rates are calculated using the procedure outlined in

reference [38]. It is known that the scattering processes in wurtzite type GaN is much different from the scattering processes in, for example, GaAs [45,46]. But these differences do not arise in zincblende type GaN so that it is sufficient to consider the usual longitudinal optic phonon-electron interaction only in the present study [46].

Remote impurity scattering calculation is based on the suggestion made in [32] where the total and induced fields are related to the self-consistently calculated wavefunctions from the solution of Poisson-Schrödinger equations. This treatment goes beyond the electric quantum limit and considers both intra and inter subband scatterings through the calculation of matrix elements that connects the external and induced potentials. Therefore the treatment of screening is of Lindhard type. The Fermi energy required for the calculation of upper limit of the electron wavevector for a particular heterostructure at a specified temperature is found during the solution of Poisson-Schrödinger equations and this value is used in the ensemble Monte Carlo transport simulations.

Finally, surface roughness scattering is calculated assuming that the variation in the potential is proportional to perturbation at the hetero interface [40–44]. An exponential form of autocorrelation function [40] for the distribution of scattering centers for surface roughness scattering is assumed. In all calculations of scattering rates the self consistently calculated wave functions from the solution of Schrödinger and Poisson equations are used. Polarization effects which has been shown to have a considerable effect on charge localization and transport properties [7–14] are completely neglected in this study, i.e. we consider a so called fully relaxed interface for AlGaN/GaN structures. The material parameters used in the calculations for GaN and $Al_xGa_{1-x}N$ are shown in Table 1.

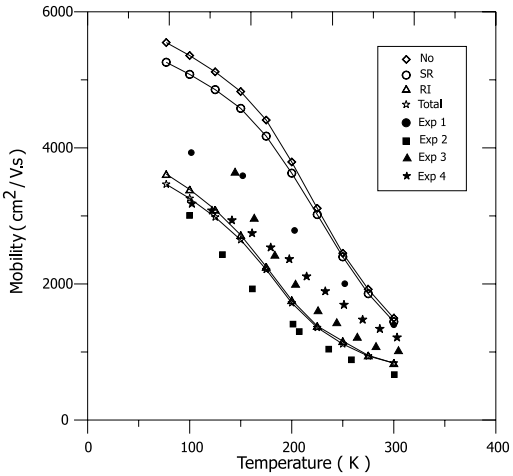

Fig. 3. Experimental and simulated electron mobility of 2D electrons confined to the AlGaN/GaN quantum well under various scattering mechanisms. Simulation result for an exponential auto correlation function is used with the parameter values of $L = 2.7$ Å, and $\Delta = 4.3$ Å. The hetero structure layer thicknesses and doping parameters are the same as given in Figure 2. The simulation mobility values when phonon (acoustic and optic) scattering is considered only is shown by diamonds. In addition to phonon scattering, the effect of surface roughness alone and ionized remote impurities alone are shown by circles and triangles, respectively. The mobility when the combined effect of phonons, remote impurities and surface roughness is considered is depicted by stars. Note that for all cases considered, electron mobility decreases considerably with temperature due to the domination of optic phonon scattering at high temperatures. Experimental results from references [12,21,50,51] are also shown. Filled circles labeled as 'Exp1' are from reference [12], filled squares labeled as 'Exp2' are from reference [21], filled triangles labeled as 'Exp3' are from reference [50], filled stars labeled as 'Exp4' are from reference [51].

3 Results and discussions

The scattering mechanisms mentioned in the previous section are considered in the ensemble Monte Carlo [47] simulation of electron transport in the quantum well. The numerical code used in the simulations essentially bases on the work presented in [47] modified in accordance with the requirements of the present study. Inter and intra sub band scattering of electrons in the quantized states in the Γ valley of GaN in the quantum well are taken into account. The number of energy levels, the electron concentrations in each level and the wave functions for each level are found from the self consistent numerical solution of Poisson and Schrödinger equations. These wave functions are used in the calculation of 2D scattering rates. All electrons are initially assumed to be in the first sub band and their evolution under an applied electric field parallel to the hetero interface is studied. As the applied field increases the energy of electrons also increases but for all field values used in this study the electrons remain in the well without transferring to the three dimensional valleys of GaN.

First we show the mobility characteristics of the 2DEG at various temperatures in Figure 3. The parameter values for the hetero junction are the same as those shown in Figure 2. The mobility curves shown in Figure 3 correspond to the mobility of 2D carriers calculated at a moderate field value of $F = 3$ kV/cm directly from the equation $\mu_e = v/F$ where v is the drift velocity of the carriers at steady state and F is the applied field. These mobility values appear to be consistent with and in the same limits as the reported experimental mobility values [12,21,50,51]. The mobility values when the effect of both remote impurities and surface roughness are neglected is shown by diamonds. The autocorrelation function for the distribution of remote impurities is assumed to be in the form of exponential function given by

$$\Delta(r) = \Delta^2 e^{-r/L} \tag{3}$$

where Δ is the root mean square (rms) value of surface roughness and L is the lateral extension of the effect of scattering center on the plane of the hetero junction. The effect of the roughness on the potential assumed to be proportional to the value of the interface roughness $\Delta(r)$ [40–44]. Surface roughness scattering is considered

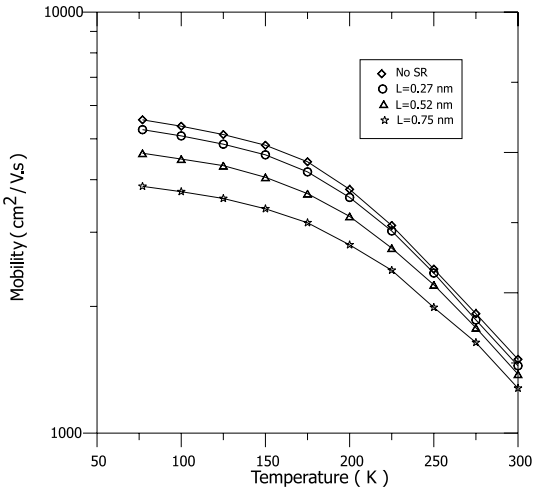

Fig. 4. Mobility of two dimensional carriers as a function of temperature at various lateral extension L of surface roughness scattering when the rms value of the roughness at the junction is $\Delta = 4.3$ Å. The parameters of the hetero junction are the same as those given in Figure 2. Remote impurity scattering is not included for the present calculation. The curve with diamonds correspond to the case when phonon scattering alone is taken into account. The effect of surface roughness on mobility is shown as a function temperature for the lateral extensions of scattering centers $L = 2.7$ (circles), 5.2 (triangles) and 7.5 (stars) Å for the case when the rms value of surface roughness is $\Delta = 4.3$ Å. Surface roughness scattering is more effective at low temperatures and as the temperature increases the effect of roughness becomes less pronounced because optic phonon scattering becomes the dominant mechanism that controls the mobility.

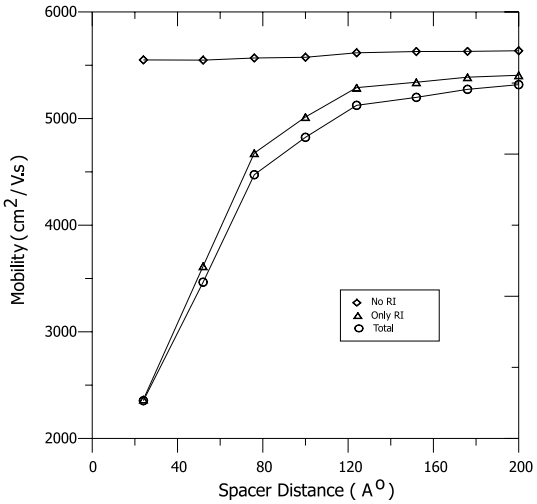

Fig. 5. Mobility of 2D carriers as a function of spacer layer thickness for various scattering mechanisms. The surface roughness parameters for the exponential auto correlation function are $L = 2.7$ Å, and $\Delta = 4.3$ Å. The parameter values for the AlGaN/GaN hetero junction are the same as given in Figure 2. except the thickness of spacer layer. The effect of phonon scattering alone is shown by diamonds. When remote impurity scattering is added the result is depicted by triangles and finally when the effect of surface roughness is also added on the mobility values is shown by circles. Remote impurity scattering is very effective for small values of w_s but its effect decreases considerably as the spacer width increases since remote impurity scattering rates decrease exponentially with spacer layer thickness.

only at the AlGaN/GaN interface on the barrier side of the junction, scattering at the junction on the substrate side is neglected. The effect of surface roughness on mobility is shown in Figure 3 by the curve with circles when the surface roughness parameters used in the calculations are $\Delta = 4.3$ Å and $L = 2.7$ Å. In addition to phonon (acoustic and optic) scattering, the effect of ionized remote impurities (without considering surface roughness scattering) when screening effects are taken into account is also shown in Figure 3 (triangles). The mobility when the combined effect of phonons, remote impurities and surface roughness is considered is depicted by stars Figure 3. Experimental results from references [12,21,50,51] are also shown in Figure 3 to compare with the simulated results. Filled circles labeled as 'Exp1' are from reference [12], filled squares labeled as 'Exp2' are from reference [21], filled triangles labeled as 'Exp3' are from reference [50], and finally filled stars labeled as 'Exp4' are from reference [51]. The agreement between the experimental and the simulated ones is satisfactory. For all cases considered as the temperature increases, the mobility decreases considerably due to the domination of optic phonon scattering at high temperatures.

Now we consider the effect of surface roughness alone on the mobility of carriers in the presence of acoustic and optical phonon scatterings, neglecting the effect of remote impurities. The effect of surface roughness on mobility is shown in Figure 4 as a function of temperature for the lateral extensions of scattering centers $L = 2.7$, 5.2 and 7.5 Å for the case when the rms value of surface roughness is $\Delta = 4.3$ Å. As one can see from the figure surface roughness scattering is more effective at low temperatures and as the temperature increases the effect of roughness becomes less pronounced because optic phonon scattering becomes the dominant mechanism that controls the mobility. In surface roughness scattering the parameter that determines the scattering ratio is the product $\Delta \cdot L$, so the same mobility values can be obtained using various combinations of Δ and L.

The dependence of mobility to the spacer layer thickness $w_s = d_2$ which separates ionized impurities from channel electrons is shown in Figure 5. Remote impurity scattering is very effective for small values of w_s but its effect decreases considerably as the spacer width increases since remote impurity scattering rates decrease exponentially with w_s [32,39]. The mobility values when scatterings due to phonons only is shown by diamonds. Besides acoustic and optical phonon scatterings, the case when there is only remote impurity scattering is shown by triangles and when both remote impurity and surface roughness scatterings are present by circles.

Next we consider the dependence of mobility on donor concentration in the AlGaN layer for a fixed value of

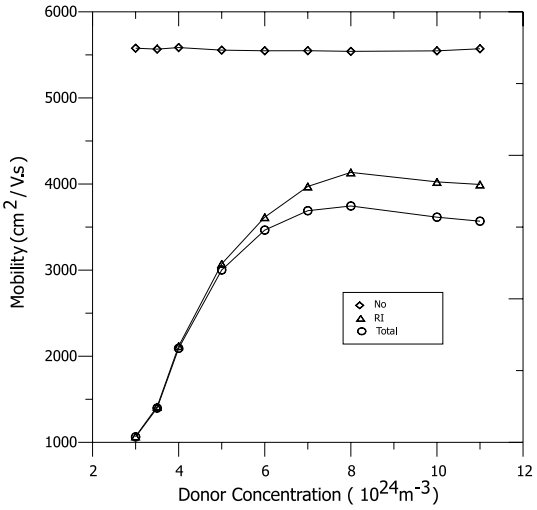

Fig. 6. Mobility of 2D carriers as a function of donor concentrations for various scattering mechanisms at a fixed spacer layer thickness. The parameter values for the AlGaN/GaN hetero junction are the same as given in Figure 2 except the donor concentrations. Surface roughness parameters are the same as given in Figure 5. Mobility of electrons when only phonon scattering is considered is shown by diamonds, when the effect of remote impurities is added by triangles and when all mechanisms including surface roughness is shown by circles. The effect of remote impurity is highest at lowest values of donor concentration because screening effects are minimal and therefore electrons are scattered by bare Coulomb potentials.

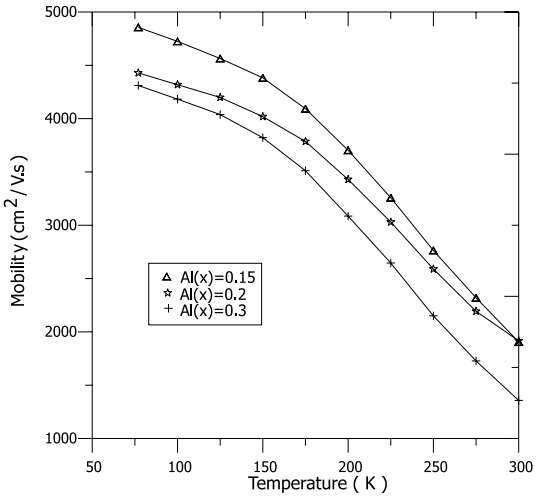

Fig. 7. The mobility of carriers as a function of temperature with Al mole fractions of 15%, 20%, and 30%. The parameter values for the AlGaN/GaN hetero junction are the same as given in Figure 2 except the Al mole fraction. Surface roughness parameters are the same as given in Figure 5.

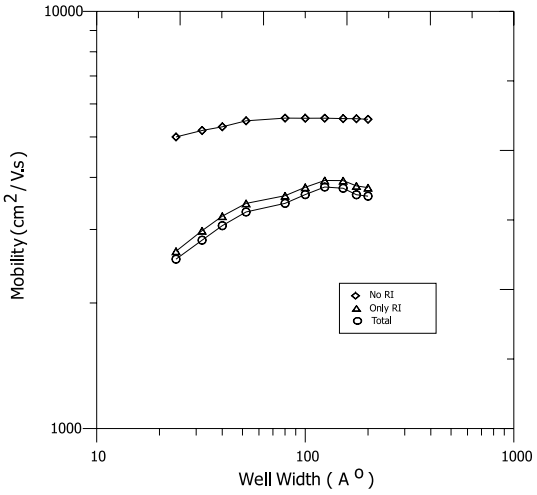

Fig. 8. The mobility of carriers as a function of well width in the absence (diamonds), in the presence (triangles) of remote impurity scattering and when surface roughness scattering is also included (circles) at 77 K. The parameter values for the AlGaN/GaN hetero junction are the same as given in Figure 2 except the well width. Surface roughness parameters are the same as given in Figure 5.

spacer layer thickness. As depicted in Figure 6, for small concentrations ionized impurities greatly reduce the mobility because the number of carriers are low at these doping concentrations and hence the effect of screening is minimal, therefore electrons interact with the impurities through bare Coulomb potentials. But as the concentration increases the level of screening also increases so that effect of donor concentration on mobility becomes less effective. But on the other hand, the effect of surface roughness increases with the increase of donor concentration. This is due to the fact that the number of two dimensional electrons confined to the hetero junction increases with donor concentration and this in turn increases the steepness of the potential near the junction. As a result the average distance of electron concentration to the interface decreases and therefore the effect of surface roughness on electron motion increases. A similar effect is also observed when the Al concentration is increased (see Fig. 7).

The effect of Al composition on mobility is also considered. The results for calculated mobility as a function of temperature with Al mole fractions x =15%, 20% and 30% are shown in Figure 7. As the Al fraction increases, the discontinuity in the barrier in the conduction band also increases. This leads to better confinement of carriers to the two dimensional hetero junction, which in turn also increases the band bending near the junction at the barrier region. This latter effect increases the role of surface roughness because the carriers are pushed towards the interface considerably which thus reduces the mobility as seen in Figure 7.

Finally we consider the effect of well width on mobility. Figure 8 shows the variation of mobility with well width in the absence (diamonds), in the presence (triangles) of remote impurity and when all scattering mechanisms are included (circles) at a temperature of 77 K. The parameter values for surface roughness scattering are: $\Delta = 4.3$ Å and $L = 2.7$ Å. Note that the decrease in mobility due to surface roughness is almost independent of the well width at the given temperature, the mobility decreases almost by the same constant amount for all well width

values. This same behavior is observed when remote impurity scattering was absent in a previous study by the same authors [17]. As one can see from the figure the effect of ionized remote impurity scattering is more effective at narrow well widths. As the well width increases, the effect of remote impurities becomes less effective. The reason for this behavior lies in the fact that for narrow wells the electron wave function is more localized and the average distance of electron distribution to the ionized impurities is smaller and hence the effect of impurities on electron motion is stronger. As the well width increases, the electron wave functions in all levels spread across the well and therefore the average distance of electron distribution from the impurities increases which thus leads to an increase of mobility as seen in Figure 8.

4 Conclusions

In this work we studied the dependence of mobility in a modulation doped AlGaN/GaN quantum well on various parameters such as temperature, well width, Al mole fraction, doping concentration, spacer layer thickness and surface roughness parameters. The drift velocity of carriers in two dimension is calculated using ensemble Monte Carlo technique. The two dimensional mobility values decreases steadily as the temperature value increases for all cases because optic phonon scattering becomes the dominant mechanism of scattering at high temperatures. Remote impurity scattering is also very effective especially at low values of spacer layer thickness. The extent of surface roughness scattering in the plane of the junction is controlled by the parameter L. As L increases, mobility values decreases considerably especially at low temperatures. The important parameter in surface roughness scattering is the product $\Delta \cdot L$, therefore the same mobility values can be obtained for a given temperature and hetero structure parameters using different values of Δ and L. Since remote impurity scattering depends on spacer layer thickness exponentially, it is highly effective for small values of layer thickness, and decreases appreciably as the spacer length increases. The donor impurity concentration also controls the mobility of 2D electrons. For low values of donor concentration, the mobility is reduced the most since screening effects are absent at low values of donor concentration and therefore electrons interact with the ions through bare Coulomb potentials. Al mole fraction of AlGaN is also an effective mobility limiting parameter. As the Al fraction increases, the height of barrier potential increases at the AlGaN/GaN hetero interface, which in turn leads to higher charge confinement in two dimensions and hence more band bending near the junction on the barrier side. As a result the electrons are pushed toward the interface more and thus an increase in surface roughness scattering and a decrease in mobility results. Finally the width of the quantum well is effective on mobility especially at small well widths where remote impurity scattering becomes important since the wave functions are localized near the junction and therefore the electrons are closer to the ionized donor impurities.

References

1. Y.C. Yeo, T.C. Chong, M.F. Li, J. Appl. Phys. **83**, 1429 (1998)
2. W.J. Fan, M.F. Li, T.C. Chong, J.B. Xia, J. Appl. Phys. **79**, 188 (1990)
3. I. Vurgaftman, J.R. Meyer, J. Appl. Phys. **89**, 5816 (2001); I. Vurgaftman, J.R. Meyer, J. Appl. Phys. **94**, 3675 (2003)
4. L. Esaki, R. Tsui, IBM research Center, Internal Research Report No. RC2418 (1969); P.Y. Yu, M. Cardona, *Fundamentals of semiconductors: physics and materials properties* (Springer, 1996)
5. R. Dingle, H.L. Störmer, A.C. Gossard, W. Wiegmann, Appl. Phys. Lett. **33**, 665 (1978)
6. S.C. Jain, M. Willander, J. Narayan, R.V. Overstraeten, J. Appl. Phys. **87**, 965 (2000)
7. L. Hsu, W. Walukiewicz, Appl. Phys. Lett. **73**, 339 (1998)
8. N. Maeda, T. Nishida, N. Kobayashi, M. Tomizawa, Appl. Phys. Lett. **73**, 1856 (1998)
9. Y. Zhang, J. Singh, J. Appl. Phys. **85**, 587 (1999)
10. I.P. Smorchkova, C.R. Elsass, J.P. Ibbetson, R. Vetury, B. Heying, P. Fini, E. Haus, S.P. DenBaars, J.S. Speck, U.K. Mishra, J. Appl. Phys. **86**, 4520 (1999)
11. N. Maeda, T. Saitoh, K. Tsubaki, T. Nishida, N. Kobayashi, Phys. Stat. Sol. (b) **216**, 727 (1999)
12. Y. Zhang, I.P. Smorchkova, C.R. Elsass, S. Keller, J.P. Ibbetson, S. Denbaars, U.K. Mishra, J. Singh, J. Appl. Phys. **87**, 7981 (2000)
13. N. Maeda, T. Saitoh, K. Tsubaki, T. Nishida, Appl. Phys. Lett. **76**, 3118 (2000)
14. O. Ambacher, B. Foutz, J. Smart, J.R. Shealy, N.G. Weimann, K. Chu, M. Murphy, A.J. Sierakowski, W.J. Schaff, L.F. Eastman, J. Appl. Phys. **87**, 334 (2000)
15. A. Khan, A. Bhattarai, J.N. Kuznia, D.T. Olson, Appl. Phys. Lett. **63**, 1214 (1993)
16. O. Ambacher, J. Smart, J.R. Shealy, N.G. Weimann, K. Chu, M. Murphy, W.J. Schaff, L.F. Eastman, R. Dimitrov, L. Wittmer, M. Stutzmann, W. Rieger, J. Hilsenbeck, J. Appl. Phys. **85**, 3222 (1999)
17. Z. Yarar, B. Ozdemir, M. Ozdemir, Phys. Stat. Sol. (b) **242**, 2872 (2005)
18. F. Stengel, S.N. Mohammad, H. Morkoç, J. Appl. Phys. **80**, 3031 (1996)
19. Y.-F. Wu, B.P. Keller, S. Keller, D. Kapolnek, P. Kozodoy, S.P. Denbaars, U.K. Mishra, Appl. Phys. Lett. **69**, 1438 (1996)
20. R. Oberhuber, G. Zandler, P. Vogl, Appl. Phys. Lett. **73**, 818 (1998)
21. X.Z. Dang, P.M. Asbeck, E.T. Yu, G.J. Sullivan, M.Y. Chen, B.T. McDermott, K.S. Boutros, J.M. Redwing, Appl. Phys. Lett. **74**, 3890 (1999)
22. E. Frayssinet, W. Knap, P. Lorenzini, N. Grandjean, J. Massies, C. Skierbiszewski, T. Suski, I. Grzegory, S. Porowski, G. Simin, X. Hu, M.A. Khan, M.S. Shur, R. Gaska, D. Maude, Appl. Phys. Lett. **77**, 2551 (2000)
23. T. Li, R.P. Joshi, C. Fazi, J. Appl. Phys. **88**, 829 (2000)
24. N. Maeda, K. Tsubaki, T. Saitoh, N. Kobayashi, Appl. Phys. Lett. **79**, 1634 (2001)
25. Y. Zhang, J. Singh, J. Appl. Phys. **89**, 386 (2001)
26. T.-H. Yu, K.F. Brennan, J. Appl. Phys. **89**, 3827 (2001)
27. T.-H. Yu, K.F. Brennan, J. Appl. Phys. **91**, 3730 (2002)
28. M. Zervos, A. Kostopoulos, G. Constantinidis, M. Kayambaki, A. Georgakilas, J. Appl. Phys. **91**, 4387 (2002)

29. B. Jogai, J. Appl. Phys. **93**, 1631 (2003)
30. S. Gökden, Phys. Stat. Sol. (a) **200**, 369 (2003)
31. http://nina.ecse.rpi.edu/shur/nitride.htm#Lei
32. G. Bastard, *Wave Mechanics Applied to Semiconductor Heterostructures* (New York, Halsted Press, 1988)
33. W.H. Press, B.P. Flannery, S.A. Teukolsky, W.T. Vetterling, *Numerical Recipes: The Art of Scientific Computing* (Cambridge, Cambridge University Press, 1986)
34. H. Tan, G.L. Snider, L.D. Chang, E.L. Hu, J. Appl. Phys. **68**, 4071 (1990)
35. G. Martin, A. Bothchkarev, A. Rockett, H. Morkoç, Appl. Phys. Lett. **68**, 2541 (1996)
36. W. Walukiewicz, H.E. Ruda, J. Lagowski, H.C. Gatos, Phys. Rev. B **30**, 4571 (1984)
37. K. Yokoyama, K. Hess, Phys. Rev. B **33**, 5595 (1986)
38. P. Harrison, Quantum Wells, *Wires and Dots* (Jonh-Wiley Sons. Ltd., England, 2000)
39. J.H. Davies, *The Physics of Low Dimensional Semiconductors* (Cambridge, United Kingdom, 1998)
40. T. Ando, A.B. Fowler, F. Stern, Rev. Mod. Phys. **54**, 437 (1982)
41. T. Ando, J. Phys. Soc. Jpn **51**, 3900 (1982)
42. H. Sakaki, T. Noda, K. Hirakawa, M. Tanaka, T. Matsusue, Appl. Phys. Lett. **51**, 1934 (1987)
43. S. Yamakawa, H. Ueno, K. Taniguchi, C. Hamaguchi, K. Miyatsuji, K. Masaki, U. Ravaioli, J. Appl. Phys. **79**, 911 (1996)
44. F. Gamiz, J.B. Roldan, J.A. Lopez-Villanueva, P. Cartujo-Cassinello, J.E. Carceller, J. Appl. Phys. **86**, 6854 (1999)
45. C. Bulutay, B.K. Ridley, N.A. Zakleniuk, Phys. Rev. B **62**, 15754 (2000)
46. C. Bulutay, B.K. Ridley, N.A. Zakleniuk, Appl. Phys. Lett. **77**, 2707 (2000)
47. K. Tomizawa, *Numerical Simulation of Submicron Semiconductor Devices* (Artech House Inc, Japan, 1993)
48. http://www.ioffe.rssi.ru/SVA/NSM/Semicond/GaN/basic.html
49. V.W.L. Chin, T.L. Tansley, T. Osotchan, J. Appl. Phys. **75**, 7365 (1994)
50. W.S. Chen, S.J. Chang, Y.K. Su, R.L. Wang, C.H. Kuo, S.C. Shei, J. Crystal Growth **275**, 398 (2005)
51. Y.-F. Wu, B.P. Keller, P. Fini, S. Keller, T.J. Jenkins, L.T. Kehias, S.P. Denbaars, IEEE Electron Device Letters **19**, 50 (1998)